ARTICLE

Revealing ultrafast vibronic dynamics of tetracene molecules with sub-8-fs UV impulsive Raman spectroscopy

Received 00th January 20xx,
Accepted 00th January 20xx

DOI: 10.1039/x0xx00000x

Takahiro Teramoto[a*], Jun Liu[b, c], Juan Du[b, d] and Takayoshi Kobayashi[e, f]

Ultrafast dynamics of tetracene molecules in THF solution were investigated using sub-8fs ultraviolet pulse lasers and *ab initio* calculations. The time trace of absorbance changes exhibited ultrafast decay with a time constant of 165 ± 10 fs because of the relaxation from a vibronically hot excited state to the potential minimum in the S_1 state. From the signals of absorbance changes in the negative time region, we obtained the electronic dephasing time of 31.27 ±1.63 fs. Inverse Fourier transform of stationary absorption spectra exhibited rapid decay with 2.1 ± 0.08 fs. From these data, we estimated the ratio of total dephasing time to homogenous and inhomogeneous broadening as 6.7% and 93.3%, respectively. Impulsive Raman spectra reflect the wave packet dynamics of vibrational modes. Although inhomogeneous broadening blurred the phase jump across the resonance peak in the spectral range, 1156 and 1680 cm^{-1} vibrational modes exhibited a phase jump from $-\pi$ to $\sim\pi$ and -0.5π to $\sim 0.5\pi$, respectively. The amplitude profiles of these vibrational modes agree with simulated vibronic progressions of combination bands. Time–frequency analysis revealed coupling dynamics between low- and high-frequency modes, where high-frequency modes are in-plane motions and low-frequency modes are out-of-plane motions. Therefore, these coupling dynamics induce symmetry-breaking of the molecular framework, which fastens the singlet fission process.

1. Introduction

With the recent development of replacing silicon with organic/inorganic materials, solar cells have progressed rapidly.[1-11] Many materials such as organic blend polymers[3] and perovskites[4] have been proposed and investigated for high photoelectric conversion efficiency (PCE) and stability at low cost. Recently, PCEs of organic thin films[5] and perovskite[6] have exceeded 18% and 25%, respectively, reaching the Shockley–Queisser limit (33%) in single-junction devices.[12] In this context, singlet fission material is one of the candidates to achieve PCE of more than 40% in single-junction cells.[7-11]

Singlet fission is a process in which a molecule in the S_1 state transfers excess energy to a neighbouring molecule in the S_0 state after photoexcitation, resulting in the formation of a triplet pair, which then dissipates as electrons and holes or is annihilated.[13-15] Because singlet fission can create a multi-exciton state from a single photon, singlet fission materials will exhibit very high PCE when used in solar cells. External quantum efficiency above 100% and internal energy conversion of up to 200% have already been reported for singlet fission solar cells.[16, 17]

Acenes are well known for showing singlet fission,[13-18] and since the first report of singlet fission in anthracene crystals in 1965,[18] many experimental and theoretical studies have been reported.[13-43] The energy relation $\mathrm{E}(\mathrm{S}_1) \geq 2\,\mathrm{E}(T_1)$ is a minimum requirement for singlet fission. In pentacene and rubrene with the energy relation of $\mathrm{E}(\mathrm{S}_1) \geq 2\,\mathrm{E}(T_1)$, singlet fission occurs on a time scale of a few femtoseconds by efficiently converting the excess energy to produce singlet fission. However, tetracene, which has $\mathrm{E}(\mathrm{S}_1)$ less than $2\,\mathrm{E}(T_1)$ by approximately 0.2 eV, exhibits both singlet fission and triplet-triplet annihilation.[21,22] Several mechanisms have been proposed to explain the singlet fission in tetracene, including the contribution of high energy levels in the S_0 state,[22] hot bands in the S_1 state,[22] entropy effects[23] and vibronic coupling.[21] Experimentally, tetracene and its derivatives, including monomers in solutions, thin films and crystals, have been investigated using resonance Raman spectroscopy,[19] time-resolved fluorescence spectroscopy,[23-26,29,31,34,42-44] transient absorption spectroscopy,[26,30-32,36,44-48] two-dimensional (2D) electronic spectroscopy[28] and impulsive Raman spectroscopy.[40] From these, it is a common insight that the contribution of molecular vibrations is important; for example, the multiple pulse excitation at 275-fs intervals improved the singlet fission

[a] *Institute for Radiation Sciences, Osaka University, 1-1 Machikaneyama-cho, Toyonaka, Osaka 560-0043, Japan.*
E-mail; teramoto@irs.osaka-u.ac.jp
[b] *State Key Laboratory of High Field Laser Physics and CAS Centre for Excellence in Ultra-intense Laser Science, Shanghai Institute of Optics and Fine Mechanics (SIOM), Chinese Academy of Sciences (CAS), Shanghai 201800, China.*
[c] *University Centre of Materials Science and Optoelectronics Engineering, University of Chinese Academy of Sciences, Beijing, China*
[d] *. Hangzhou Institute for Advanced Study, University of Chinese Academy of Sciences, Hangzhou 310024, China*
[e] *Advanced Ultrafast Laser Research Centre and Brain Science Inspired Science Support Centre, The University of Electro-Communications, 1-5-1 Chofugaoka, Chofu 182-8585, Tokyo, Japan*
[f] *Department of Electrophysics, National Chiao-Tung University, Hsinchu 300, Taiwan*

†Electronic Supplementary Information (ESI) available: Calculated vibrational modes of tetracene. Simulated IR absorption spectra, Shift vectors and Huang Rhys factors , Duschinsky matrix, figures of vibrational modes of tetracene, simulated vibronic spectra of tetracene with and without Duschinsky matrix, real time trace of ΔA in full time scale ,fitting results of perturbed free induction decay signals, and spectrograms are described. See DOI: 10.1039/x0xx00000x

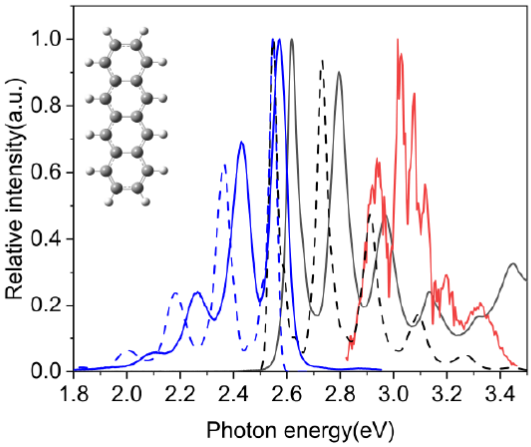

Fig. 1 Stationary absorption spectra (black line) and fluorescence spectra (blue line) of tetracene in THF solution. The simulated stationary absorption spectra(black dot) and fluorescence spectra(blue dot) due to TDDFT calculations. Laser spectra (red line). All spectra are normalised. The molecular structure of tetracene is displayed in the inset of the figure.

yield by approximately 20%,[35] and resonance Raman experiments have also suggested that high and low frequency vibrational modes couple during internal conversion.[19] However, to the best of our knowledge, there are no reports that directly observe the vibronically hot state in the S_1 state in tetracene with the ultrashort time scale after photoexcitation.

We have constructed sub-8-fs pulse laser in the ultraviolet (UV) region and used them in pump–probe experiments.[49-51] In addition, with the advance of *ab initio* calculations, it has become easier to interpret the experimental evidence by theoretical simulations.

Here, we show the ultrafast spectroscopy of tetracene in Tetrahydrofuran (THF) solution using a sub-8-fs UV pulse laser, along with *ab initio* calculations, to reveal the ultrafast dynamics of tetracene molecules in vibronically hot states in the S_1 state.

2. Experimental

The experimental details have been described in previous studies.[49-51] The outputs of the regenerative amplifier system (800 nm, 2.5 mJ and 25 fs, Legend Elite, Coherent Inc.) were used to generate 400 nm pulses by the second-harmonic generation in a BBO crystal. The 400 nm pulses were guided to the Ar-filled hollow core fibre (length: 60 cm, Ar pressure: 0.8 atm) to broaden the spectra. The output pulse width was reduced to ~7.5 fs using a pulse compressor system composed of a prism pair and a grating-deformable mirror system.[50] The ultrashort UV pulses were divided into pump and probe pulses to perform ultrafast spectroscopy, keeping the stability over 3 hours[49-51]. The delay time between the pump and probe pulses was controlled by a 10-nm-resolution feedback stage (FS-1020X, Sigma Tech, Inc.). Both pump and probe pulses are focused on the sample with pulse energies of 36 and 3.6 nJ, respectively. The transmitted probe pulse was spectrally dispersed using a polychromator (SpectraPro2300i, Acton Research, Inc.) and guided to the 128-channel lock-in amplifier system (7210/90, Ametek Inc.) through a custom-made 128-bundle fibre (Fiber Tech Optica, Inc.). The spectral range used in this study was 359–440 nm (corresponding to the photon energy range of 2.82–3.45 eV with a resolution of ~1.5 nm).

A commercially available tetracene sample (sublimed grade, Sigma-Aldrich Inc) was used without purification. The tetracene was dissolved in THF solution(0.65mM).The sample was measured with 1mm thick cell. Stationary absorption and fluorescence spectra were recorded using an absorption spectrometer (Shimadzu, UV-3101PC) and a fluorophotometer (Hitachi, F-4500), respectively.

Time-dependent density functional theory calculations of tetracene molecules have been performed in the BMK/aug-cc-pvdz level with a polarised continuum model in THF solution using the Gaussian16 package.[52]

3. Results and discussion.

3.1 Stationary absorption spectra of tetracene

Fig. 1 shows the stationary absorption spectra of tetracene in THF solution. The absorption peak at 0–0 transition from the S_0 ($^1A_{1g}$) to S_1 ($^1B_{2u}$) states appears at 2.62 eV.In the photon energy range overlapped with the laser spectra, the maximum absorbance is 0.9 at 2.97eV in this study. The discrete vibronic progressions appear at 2.80, 2.97 and 3.13 eV. The energy differences between neighbour double bands are 0.177 eV (1428 cm^{-1}), 0.174 eV (1404 cm^{-1}) and 0.161 eV (1301 cm^{-1}). The peaks corresponding to the transitions from the S_0 ($^1A_{1g}$) to S_2 ($^1B_{1g}$) states appear above 3.3 eV, overlapping with the higher vibronic states in the S_1 state.

The fluorescence spectra also exhibit vibronic progressions with the mirror symmetry to the absorption spectra. The energy difference of 0–0 transition peaks between absorption and fluorescence spectra is 68 meV, indicating that the Stokes shift due to the solvation is considerably small.

The TD-DFT calculation (black dot line) without scaling reproduces the stationary absorption spectra well. The energy difference in the 0–0 transition between the experiment and theory is 70 meV. The assignment of the composed vibrational modes in the vibronic spectra is described in the theoretical section in detail.The simulated fluorescence spectra also reproduces the experimental results well. In that sense, the excited state dynamics such as mode mixing during the transition and reorganization due to solvent can be described well. Therefore, we concluded that the theoretical calculation level and basis set used in this study is valid.

The laser spectra (red line) used in this study are also depicted in Fig. 1. We observed the ultrafast dynamics of tetracene molecules with higher vibronically excited states in the S_1 state.

3.2 *Ab initio* calculations of tetracene molecules

Before analysing the results of the impulsive Raman study of tetracene, we would like to introduce the quantum chemical calculation results. DFT calculations of tetracene molecules in THF solution have been performed to clarify the vibronic coupling in the S_0–S_1 transition.

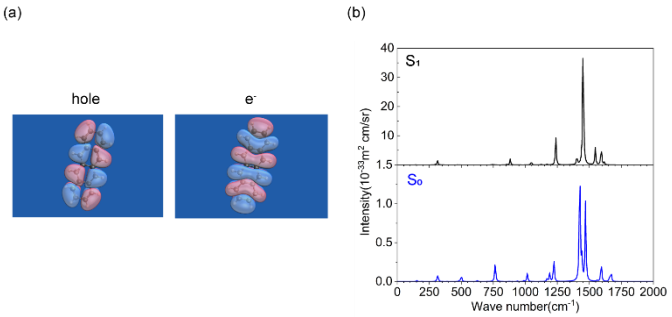

Fig. 2 (a) NTO pair of the transition from the S_0 to S_1 states in tetracene. (b) Simulated Raman spectra of tetracene in the S_0 (black) and S_1 states (blue). Spectra range is limited to 2000 cm^{-1}.

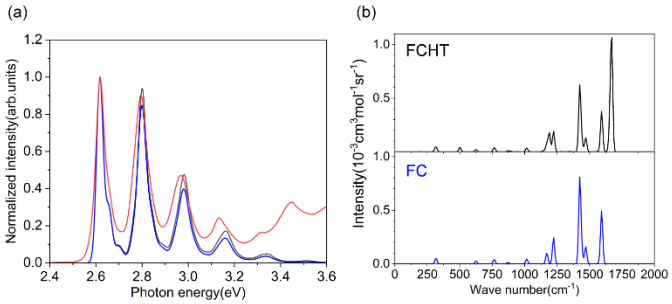

Fig. 3 (a) Simulated vibronic spectra with FC(blue) and FCHT (black) approximation and experimental stationary absorption spectra(red)(b)Simulated resonance Raman spectra with FC (blue) and FCHT(black) approximation. Excitation photon energy is 3.13eV.

Natural transition orbital (NTO) analysis was performed for the S_0–S_1 transition in tetracene.[60] NTOs provide a compact and state-specific description of the excitation. The morphology of the NTO pair in the transition is depicted in Fig. 2(a). It is found that the NTOs are almost composed of HOMO/LUMO orbitals(>98%).The nodes exist in-plane and parallel to the short axis in the plane of tetracene in both hole and electron NTOs, showing the $\pi \longrightarrow \pi^*$ character in the transition from the S_0 to S_1 states.[15]

Tetracene has 84 vibrational modes, and because of the highly symmetric D_{2h} structure, the vibrational modes exhibit infrared (IR)–Raman alternative selection rules. Frequency analysis of tetracene in the S_0 and S_1 states in THF solution has been performed. All vibrational modes are listed in the †ESI. Raman spectra of tetracene in the S_0 and S_1 states without scaling are shown in Fig. 2(b) (IR spectra are depicted in †ESI). The spectra computed by DFT are simply the off-resonant Raman spectra ,not resonance Raman. Raman signals appear at 317, 501, 765, 1016, 1190, 1223, 1425, 1471, 1593 and 1670 cm^{-1} in the S_0 state, whereas they appear at 314, 882, 1047, 1238, 1400, 1451, 1546 and 1593 cm^{-1} in the S_1 state. These modes belong to the total symmetric A_g character in the D_{2h} point group, except 501, 1190 and 1670 cm^{-1} belonging to B_{3g}. Using these data, we can generate vibronic absorption spectra and resonance Raman spectra.

Table 1 Simulated transition tables at 2.90 and 309 eV.

Vibronic transition	Transition energy(eV)	Line intensity (normalized to 0-0 transition intensity)
	2.90 eV	
$\|1\rangle^2 \rightarrow \|62'\rangle^1\|59'\rangle^1\|1'\rangle^2$	2.9013	0.0490
$\|2\rangle^1 \rightarrow \|62'\rangle^1\|59'\rangle^1\|2'\rangle^1$	2.9013	0.0526
$\|1\rangle^1 \rightarrow \|62'\rangle^1\|59'\rangle^1\|1'\rangle^1$	2.9018	0.0631
$\|0\rangle \rightarrow \|62'\rangle^1\|59'\rangle^1$	2.9023	0.0809
$\|0\rangle \rightarrow \|62'\rangle^2$	2.9083	0.0487
$\|0\rangle \rightarrow \|68'\rangle^1\|59'\rangle^1$	2.9141	0.0495
$\|0\rangle \rightarrow \|68'\rangle^1\|62'\rangle^1$	2.9201	0.0515
	3.09 eV	
$\|0\rangle \rightarrow \|62'\rangle^1\|59'\rangle^2$	3.0763	0.0094
$\|2\rangle^1 \rightarrow \|62'\rangle^2\|59'\rangle^1\|2'\rangle^1$	3.0813	0.0086
$\|0\rangle \rightarrow \|62'\rangle^2\|59'\rangle^1$	3.0823	0.0132
$\|0\rangle \rightarrow \|66'\rangle^1\|62'\rangle^1\|59'\rangle^1$	3.0895	0.0088
$\|2\rangle^1 \rightarrow \|68'\rangle^1\|62'\rangle^1\|59'\rangle^1\|2'\rangle^1$	3.0931	0.0099
$\|0\rangle \rightarrow \|68'\rangle^1\|62'\rangle^1\|59'\rangle^1$	3.0941	0.0152
$\|0\rangle \rightarrow \|70'\rangle^1\|62'\rangle^1\|59'\rangle^1$	3.0999	0.0084

The transition dipole moments can be expanded in the Taylor expansions, as follows:

$$\mu(Q)=\mu_0(Q) + \sum_{k=1}^{N}\left(\frac{\partial}{\partial Q_k}\mu\right)_0 Q_k'' + \cdots. \quad (1)$$

The truncation only to the first term is called Franck–Condon (FC) approximation, and the case including the second term is Hertzberg–Teller (HT) approximation. Because the HT effect appears in acenes[24,27] and the highly symmetric molecules,[61] we calculated and compared both the FC and FCHT approximations through the simulation of vibronic spectra and simulated resonance Raman spectra.

Fig. 3(a) shows vibronic spectra with the FC and FCHT approximations.For the comparison, the photon energies of 0-0 transition and its intensities in the simulated vibronic spectra with FC and FCHT approximations are scaled to the experimental data . The transition intensities in the vibronic progression are slightly different between the FC and FCHT approximations. The intensity of the 0–0 transition is slightly higher in the FCHT approximation than in the FC approximation, but others show a reverse relation. The transition energies are the same as expected. Fig. 3(b) shows resonance Raman spectra at an incident photon energy of 3.13 eV, which is a similar condition to the resonance Raman spectroscopy of tetracene, except for the solvent.[19] From the figure, the resonance Raman spectra in the FCHT approximation appear at 504, 1192 and 1672 cm^{-1}, whereas these are not observed in the FC approximation. These modes belong to B_{3g} symmetry and are experimentally observed in resonance Raman spectroscopy,[19] indicating that the FCHT approximation is appropriate in the transition from the S_0 to S_1 states in tetracene.

The vibronic spectrum with the FCHT approximation was simulated by the convolution of the Gaussian distributions of the vibronic progressions with full width at half maximum bandwidth of 135 cm^{-1} at 300 K.[62] Because the simulated vibronic spectra reproduce experimentally observed stationary absorption spectra well, we focus on the vibronic progressions obtained from *ab initio* calculations. The vibronic progressions with their transition energies and intensities are shown as the stick bars in the simulated vibronic spectrum (Fig. 4(a)). There are two typical peaks centred at 2.90 and 3.09 eV in the simulated stationary absorption spectrum. The top seven transitions from the highest intensity at each peak are listed in Table 1. The labels of $|i\rangle$ and $|i'\rangle$ (i and i' correspond to the

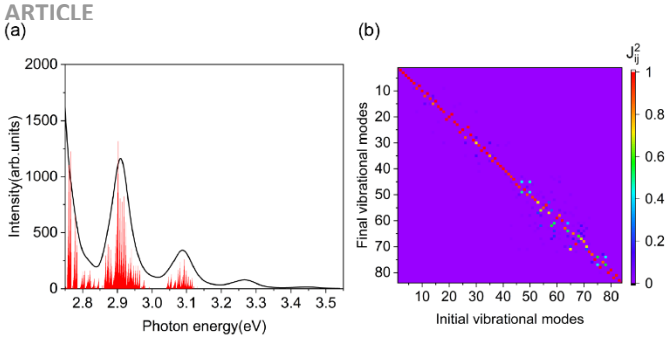

Fig. 4 (a) Simulated vibronic spectrum (black) and their components with each vibronic transition (red). (b) Duschinsky matrix of the transition from the S_0 to S_1 states in tetracene.

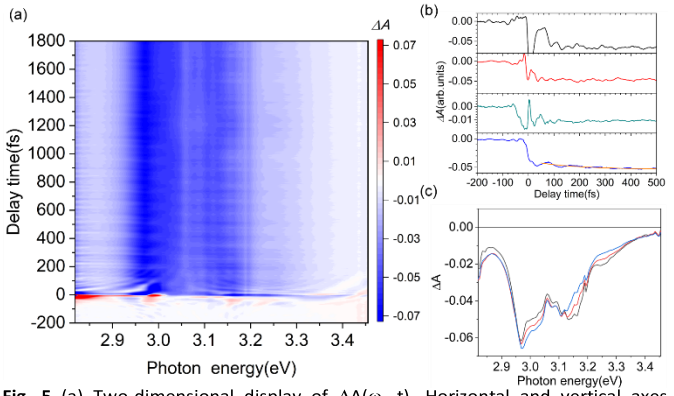

Fig. 5 (a) Two-dimensional display of ΔA(ω, t). Horizontal and vertical axes correspond to the probe photon energy and delay time, respectively. The colour represents ΔA. (b) Real-time trace of ΔA(ω, t) with photon energy at 2.968(black) 3.134(red), 3.319(green), and 3.029 (blue).The exponential fitting with time constant of 165fs is plotted (orange) (c) Time-resolved ΔA(ω, t) with the delay time of 200 (black), 500 (red) and 1000 fs (blue).

vibrational mode number in the Sp_0 and S_1 states, respectively) are used to label the vibrational modes listed in † ESI. High-frequency Raman active vibrational modes such as $|59'\rangle$, $|62'\rangle$, $|66'\rangle$, $|68'\rangle$ and $|70'\rangle$ (corresponding to 1403, 1451, 1510, 1546 and 1593 cm^{-1}, respectively) exhibit the combination bands in both peaks. Low-frequency vibrational modes such as $|1'\rangle$ and $|2'\rangle$ (corresponding to 47 and 81 cm^{-1}, respectively) can couple these combination bands with their hot bands depending on the population at the temperature. Comparing the two peaks at 2.90 and 3.09 eV, there are two combinations of high-frequency modes at the 2.90 eV peak, for example, $|0\rangle \rightarrow |62'\rangle^1|59'\rangle^1$ transition at 2.902 eV. Meanwhile, there are three combinations at the 3.09 eV peak, such as $|0\rangle \rightarrow |62'\rangle^2|59'\rangle^1$ at 3.0759 eV. According to previous studies, these vibrational progressions in the stationary absorption spectra are simple overtones of a single vibrational mode.[19,25,30] However, our simulation indicates that the complex combination bands are involved in the stationary absorption spectra.

The differences in the location of the minimum and the curvature of the potential energy surface between the S_0 and S_1 states induce the displacement and rotation of the coordinates of normal modes. These are described as the shift vector and Duschinsky matrix.[62] The vibrational modes with large shift vectors are listed in Table 2. The shift vector is the geometry shift (displacement) from initial to final state equilibrium geometries expressed in the mass-weighted normal coordinates of the initial state (the dimension is Bohr $\times \sqrt{m_e}$,

Table 2 Simulated reorganisation energies for Raman active modes of tetracene

vibrational mode	wavenumber (cm^{-1})	Shift Vector (atomic units)	Huang-Rhys Factor	Reorganization energy (cm^{-1})
8	317.2266	19.1527	0.2651	84.2719
20	625.4183	-4.7905	0.0327	20.4930
25	765.3405	-4.7333	0.0391	29.9553
44	1016.1288	2.3515	0.0128	13.0330
48	1170.9141	-5.2859	0.0745	87.4467
52	1222.8035	-7.0369	0.1379	169.0184
60	1425.1554	-11.2344	0.4098	585.1800
61	1441.8098	3.7612	0.0465	67.1379
64	1470.6604	5.2725	0.0931	137.2574
68	1593.1378	7.9631	0.2301	367.3944

where m_e is the electron mass). Huang–Rhys factors S_i of the i-th vibrational mode ω_i is related to the shift vector Δ_i as $S_i = \omega_i/2\Delta_i^2$. The reorganisation energy λ_i was calculated using Huang–Rhys factors ($S_i = \lambda_i/\hbar\omega_i$). These values are almost consistent with the previous resonance Raman study.[19]

Fig. 4(b) shows the contour map of the Duschinsky matrix. The index in the bottom is the initial (ground) state, and the left corresponds to the vibrational modes in the electronically excited state. The order of vibrational modes depends on the vibrational frequency. The off-diagonal peaks in the figure indicate that the order of vibrational modes is changed or that mode mixing among vibrational modes occurs during the transition. The typical diagonal and off-diagonal contents of the Duschinsky matrix are listed in † ESI. As mentioned before, the mode mixing happens due to the displacement (shift vector) and rotation of the coordinates (Duschinsky matrix). To evaluate the contribution of Duschinsky matrix in the mode mixing, we simulated the vibronic spectra with and without Duschinsky matrix (Fig. S3). The overall shape of absorption spectra can be reproduced well even without Duschinsky matrix.Comparing the simulated results, we found that the simulated spectra without Duschinsky matrix overestimates the intensity distributions above 0-0 transition rather than the spectra with Duschinsky matrix. Anyway, we concluded the mode mixing happens mainly due to the large displacement (shift vector). These induce the combination bands that appear in the simulated stationary absorption spectra.

3-3.Ultrafast spectroscopy of tetracene in THF solution

3-3-1. Excited state dynamics of tetracene in the positive time range

Fig. 5(a) displays 2D transient absorption spectra $\Delta A(\omega, t)$ of tetracene molecules. The time traces of ΔA at probe photon energies of 2.97, 3.13 and 3.3 eV and ΔA at delay times of 200, 500 and 1000 fs were depicted in Figs. 5(b) and (c), respectively. From the figure, $\Delta A(\omega, t)$ has a negative value because of photobleach in mostly the entire spectral domain in the positive time regime.

However, around the 3.13eV peak, we found a rapid decay in the time trace of $\Delta A(\omega, t)$. To analyse the dynamics, we fitted $\Delta A(\omega, t)$ with a single exponential decay($\Delta A(\omega, t) = A \times$

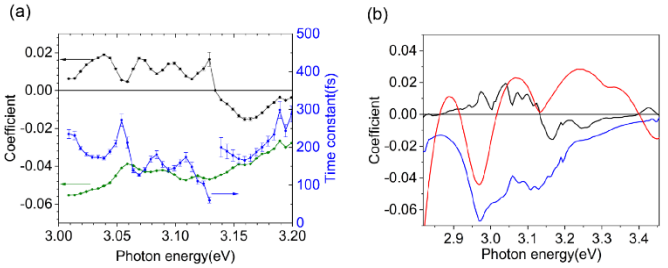

Fig. 6 (a) Probe photon energy dependence of the fitting results with single exponential decay to ΔA(ω, t). The coefficients of decay(*A*) and constant(*c*) components (black and green, respectively) and time constants (blue) are shown with respect to the photon energy. The error bars are involved. (b) Decay-associated spectra. The fast and slow decay components (black and blue, respectively) with respect to the photon energy are shown. The reverse of stationary absorption spectra is also shown (red).

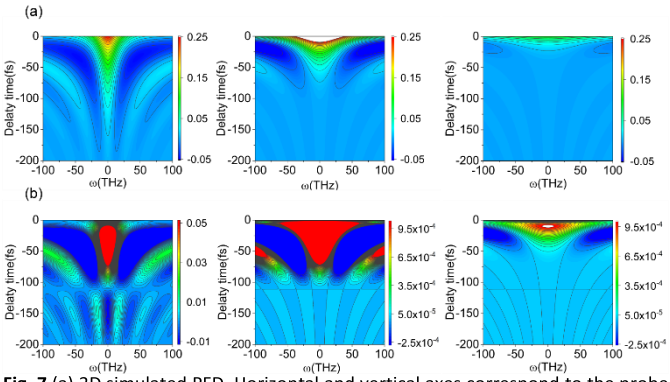

Fig. 7 (a) 2D simulated PFD. Horizontal and vertical axes correspond to the probe photon energy and delay time, respectively. The electronic dephasing times used in the simulation are 50, 20 and 10 fs, respectively, from the left to right in the panel. (b) Simulated PFD spectra with the modulation of molecular vibration (ω_v = 150cm^{-1},ϕ =π/2). The electronic dephasing times are the same as (a).

$exp(-t/\tau) + c$, c: $constant$). The resultant photon energy dependence of the time constants and their coefficients(*A* and *c*) are depicted in Fig. 6(a). Both time constants and their coefficients sensitively depend on the photon energy because of the damping effect due to vibronic coupling. The constant of the decay component(*A*) shows zero at the photon energy of 3.134eV. Considering the photon energy region above 3.134eV, the probe photon energy dependence of *A* is similar to that of time constants. At 3.159eV, the absolute value of *A* becomes maximum and its time constant shows 165fs. When we see the time constants in the photon energy region below 3.134 eV, it also shows 165fs at the same absolute value of *A*. Therefore, benefiting from a large signal size and long-time constant, the time constant of rapid decay could be determined as 165 ± 10 fs with reasonable precision.

Based on this value, the global fitting to the experimental data with a single exponential decay, along with a constant, was applied, and the decay-associated spectra (DAS) were reconstructed (Fig. 6(b)). The fast decay component in DAS shows first derivative-like spectra peaked at 3.13 eV in the stationary absorption spectra. It is possible that the negative ΔA observed in this study is due to stimulated emission from higher lying state to lower state, not S_1-S_0 state as observed in fluorescence spectra. However as can be seen the DAS spectra of 165fs component, the spectral shape seems first derivative like of stationary absorption spectra. From this, we concluded that the rapid decay with a time constant of 165 fs is due to the relaxation from hot vibronic states to the potential minimum in the S_1 state. *Ab initio* calculation indicated that the maximum overlap in Franck- Condon happens at photon energy of 2.87eV(70meV is added to the theoretical value).Therefore, the photon energy region in this study is above FC region. The density of state of vibrational manifolds in S_0 state is less effective in this higher energy region. And also, the effect due to S_2 state is less because the photon energy is low enough. Additionally, as seen in Fig.1, the solvation is quite small, indicating that the interaction between tetracene and its surrounding THF molecules is small. Therefore, we could find the vibronically not cooling state with long lifetime with 165fs in hot S_1 state.The same kind of relaxation in the S_1 state has been reported previously. [53,54] The other vibronic states such as the 2.97eV peak in the stationary absorption spectra are thought to relax faster than 50 fs because we could not analyse the data due to the strong coherent artefact in regions shorter than 50 fs. The constant component spectra in DAS show the reversed shape of the stationary absorption spectra, but the bandwidth is significantly broader than that of the stationary absorption spectra. This spectral difference indicates that the vibronically hot states are created in the S_1 state after photoexcitation.

3-3-2. Electronic dephasing dynamics of tetracene molecules in solution

In the 'negative' time region (probe pulse precedes pump pulse) in the transient absorption spectra, the polarisation created by the probe pulse is kicked to the pump laser fields. This process is called a perturbed free-induction decay (PFID)[55-57], and we reported the extended interpretations of PFID when using few-cycle pulses.[58-61] In these reports, we mentioned that because the pulse duration of the laser pulse is sufficiently short compared with both electronic dephasing time and molecular vibrational periods, the observed electronic dephasing time is not entirely electronic but a vibronic dephasing time.

The PFID in the two-level system is described as follows[56]:

$$\Delta T(t,\omega) \propto \exp\left(-\frac{t}{T_2}\right)\frac{[cos(\varpi-\varpi_0)t-T_2(\varpi-\varpi_0)sin(\varpi-\varpi_0)t]}{(\varpi-\varpi_0)^2+\left(1/T_2\right)^2}, \quad (2)$$

where T_2 represents the effective dephasing time and ϖ_0 represents the peak photon energy of hole burning. By modulating PFID based on molecular vibration, Eqn. (2) can be modified as follows,

$$\Delta T(t,\omega) \propto cos(\varpi_v t+\phi)\exp(-t/T_2)\times \frac{[cos(\varpi-\varpi_0)t-T_2(\varpi-\varpi_0)sin(\varpi-\varpi_0)t]}{(\varpi-\varpi_0)^2+\left(1/T_2\right)^2}. \quad (3)$$

Here, the modulation due to the molecular vibrational mode with frequency ϖ_v and initial phase ϕ is considered. Figs. 7(a) and (b) show PFID spectra with the electronic dephasing time T_2 of 50, 20 and 10 fs, with/without modulation due to the molecular vibration of 150 cm^{-1} with 0.5π. The spectra show hyperbolic features, which are typical in PFID. However, the feature seems less effective when T_2 decreases. Typical features

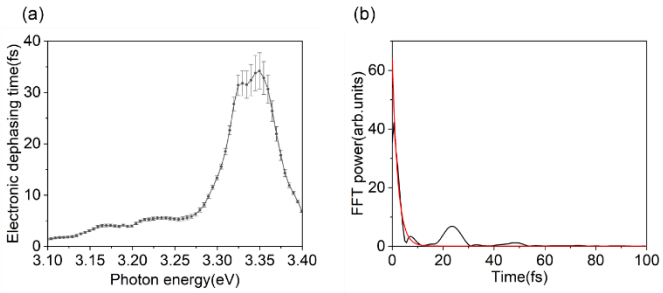

Fig. 8 (a) Probe photon energy dependence of the electronic dephasing time. (b) Inverse Fourier transform of the stationary absorption spectra of tetracene.

in vibronic PFID include a signal exhibiting oscillations because of the molecular vibrations with node and reverse signs in the time trace, in addition to the hyperbolic feature of PFID.

$\Delta A(\omega, t)$ signals in the negative time region (Fig. 5(a)) with the photon energy region of ~3.0–3.4 eV exhibit hyperbolic features. By fitting $\Delta A(\omega, t)$ signals with a convolution between instrument function assuming a Gaussian distribution with 7.5fs FWHM and a single exponential decay function (see SI), the photon energy dependence of the vibronic dephasing time is obtained (Fig. 8(a)). The dephasing time is not a constant but a structured feature. Because of the modulation due to molecular vibrations and overlapping of the PFID signals originating from consecutive peaks, the vibronic dephasing time does not remain constant in the entire spectral range. However around the peak at 3.33eV,the electronic dephasing time shows almost constant within error bar and longest dephasing time.Therefore, we determined the electronic dephasing from the average value, 31.27 ±1.63fs.

The dephasing rate $1/T_2^e$ is composed of three components, as follows:

$$\frac{1}{T_2^e} = \frac{1}{2T_1^e} + \frac{1}{T_2'^e} + \frac{1}{T_2^{*e}}, \quad (4)$$

where T_1^e represents the population decay term, and $T_2'^e$ and T_2^{*e} represent the pure electronic dephasing time and electronic phase relaxation time due to the inhomogeneous broadening, respectively. For simplicity, we estimated T_2^{*e} to be significantly longer than the other time constants from the significantly broader electronic spectrum of the ground state, i.e. $T_2^{*e} = \infty$. From the analysis of the time trace of $\Delta A(\omega, t)$ in the negative time region, we determined T_2^e as 31.27 fs. From the time trace of $\Delta A(\omega, t)$ in the positive time region, population decay from the S_1 to S_0 states is longer than 1.8 ps, which is the longest delay time in this study. Therefore, we estimated the pure dephasing time to be $T_2'^e$ = 31.27 ± 1.63 fs using Eqn. (4).

Fig. 8(b) shows the inverse Fourier transform of stationary absorption spectra of tetracene. It shows a damping oscillator with a peak at 24.3 fs (corresponding to the molecular vibration of 1430 cm^{-1}). By fitting the single exponential decay to the rapid decay component in the spectra, the total (homogenous + inhomogeneous) dephasing time is determined as 2.1 ± 0.08 fs. From these electronic dephasing times, the contributions from homogenous and inhomogeneous dephasing to the total dephasing time are 6.7% and 93.3%, respectively.

3-3-3. Wave packet dynamics of tetracene in THF solution

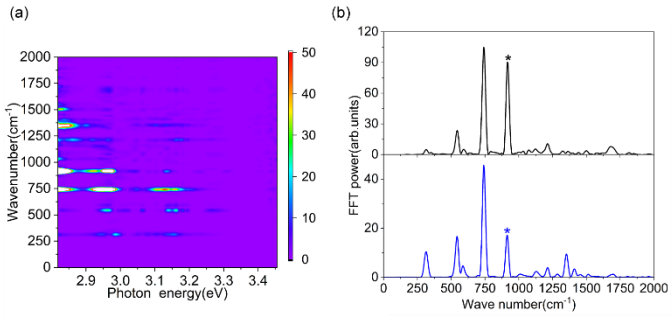

Fig. 9 (a) Fourier transform spectra of ΔA(ϖ,t). (b) FFT power spectra at photon energy of 2.96 (black) and 3.13 eV (blue).Asterisk shows the vibrational mode of THF solution

Two-dimensional fast Fourier transform (FFT) power spectra of $\Delta A(\omega, t)$ spectra are shown in Fig. 9(a). In FFT, we used a Blackman window to $\Delta A(\omega, t)$ spectra in the time range from 50fs to 1800fs with zero padding of 2^{13}.The FFT power spectra at photon energies of 2.96 and 3.13 eV are shown in Fig. 9(b). The vibrational modes with 317, 545, 740, 1034, 1156, 1217, 1347, 1408, 1505 and 1680 cm^{-1} appeared with the precision of 4 cm^{-1}. The strong peak at 915 cm^{-1} is due to THF solution(labelled with asterisk). These values are consistent with the simulated Raman spectra. Especially, 545, 1156 and 1680 cm^{-1} corresponding to 504, 1192 and 1672 cm^{-1},

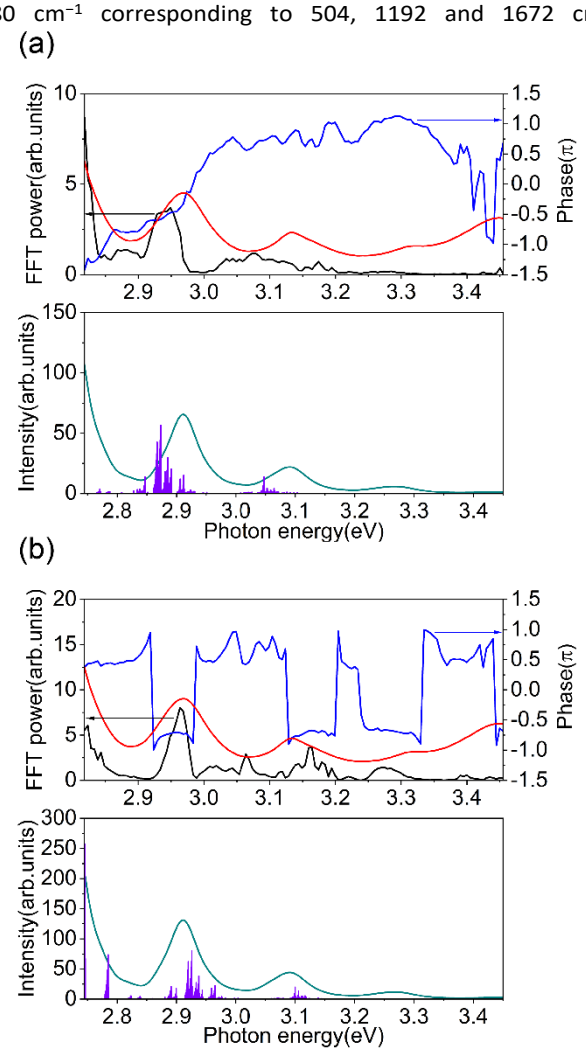

Fig. 10 (a)Stationary absorption spectra (red) and photon energy dependence of FFT power spectra (black) and phase (blue) of 1156 cm^{-1} mode (top). Simulated vibronic spectra (green) and transition intensity of combination bands of |48′⟩ modes (bottom). (b) Same as (a) but 1680 cm^{-1} mode (top) and |70′⟩ (bottom).

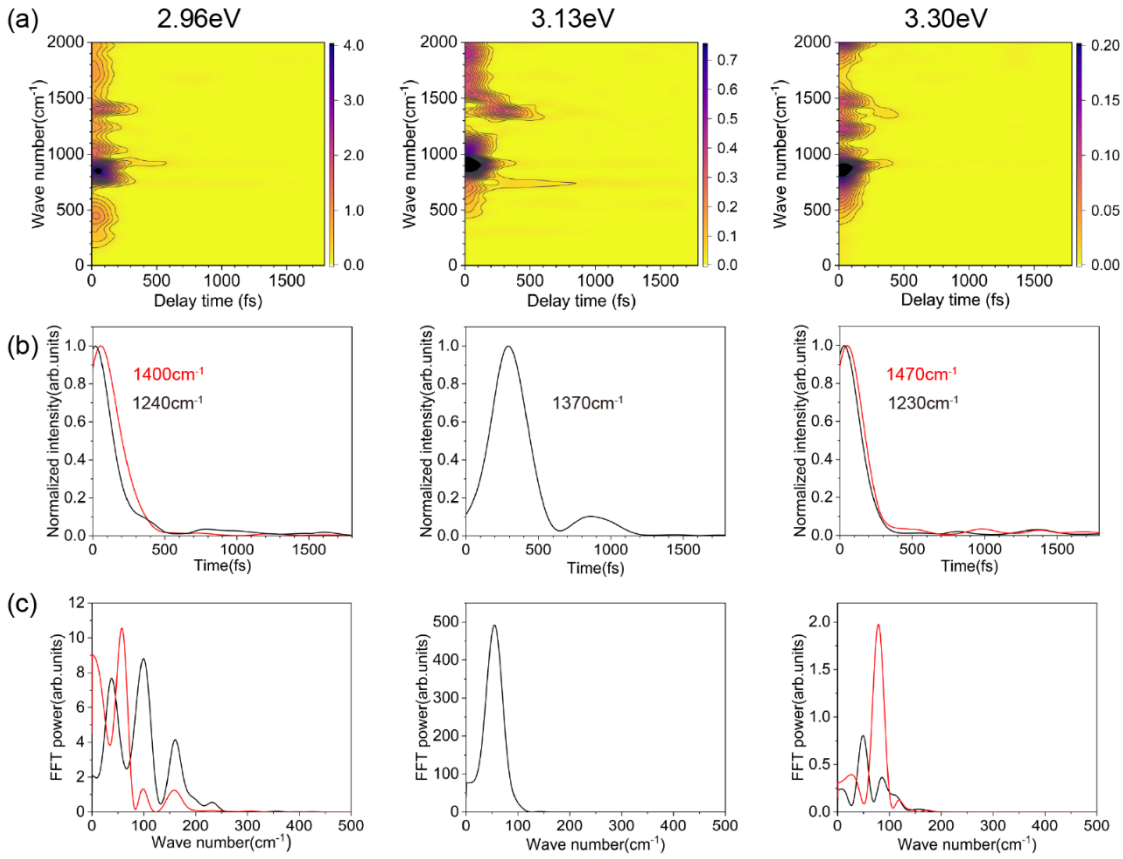

Fig. 11 (a) Spectrogram of ΔA(ϖ,t) at photon energies of 2.96, 3.13, and 3.30 eV, respectively. (b) Time trace of instantaneous maximum intensity in the spectrogram (c) FFT spectra of (b).

respectively, in simulated resonance Raman spectra with the FCHT approximation are found. This indicates that the impulsive Raman spectroscopy of tetracene directly observes the FCHT effect. And also, these vibrational modes are consistent with the simulated vibrational mode in S_0 state(see SI). These are reasonable because $\Delta A(\omega, t)$ shows negative value due to photobleach.

The dynamics of wave packets in the ground state and/or excited state induced by ultrashort pulses are reflected in the probe photon energy dependence of the amplitude and phase of the vibrational modes.[65-69] However, the ambiguity of the estimated phase is significant in low-frequency vibrational modes. For example, if the period of 317 cm^{-1} is 94.6 fs and the observed time range in this study is 1.8 ps, the accuracy of the phase becomes as large as 0.1π even with relatively high precision. Therefore, we analysed only high-frequency modes.

The ideal photon energy dependence of amplitude and phase exhibits a dip at the resonance position in the amplitude profile with a phase jump of π or 2π depending on the wave packets created in the ground state or excited state.[65,66] This feature has been observed in experiments.[67-74] However, as the contribution of inhomogeneous broadening increases, the dip in amplitude disappears and the phase jump blurs or shifts.[65,66] In this study, because we mentioned in Section 3.3.2 that the contribution of inhomogeneous broadening is sufficient, several vibrational modes such as 1217, 1347 and 1408 cm^{-1} do not exhibit a clear phase jump. Only 1156 and 1680 cm^{-1} exhibit a phase jump around the 2.96 and 3.13 eV peaks in the stationary absorption spectra, respectively (Fig. 10). The amplitude profiles show a peak and phase change from $-\pi$ to ~π and -0.5π to ~0.5π in the 1156 and 1680 cm^{-1} vibrational modes, respectively, at around the 2.96eV peak. Indeed, the amplitude profile does not exhibit a dip at the peak position. However, when we extract the combination bands involving $|48'\rangle$ and $|70'\rangle$ modes for 1156 and 1680 cm^{-1}, respectively, from the simulated vibronic transition tables, as shown in the bottom panel in Fig. 10, they seem consistent with the experimentally observed amplitude profiles. The theoretical models described by Kumar *et al* in refs.65 and 66 come from a line shape function with a single vibrational mode with damping factors. Although it can be extended to multi-mode cases, it does not consider mode-mixing dynamics. Meanwhile, at the 3.13 eV peak, 1156 cm^{-1} exhibits a constant phase across the peak, indicating its off-resonance nature. The 1680 cm^{-1} vibrational mode exhibits the same resonance feature as that at 2.96 eV.

3-3-4. Mode coupling dynamics in tetracene

Time–frequency analysis of transient absorption spectra reveals the vibrational dynamics in real time. Spectrogram analysis has been done with the condition of a time step of 10fs , Blackmann window of 280fs FWHM window width and zero padding of 2^{13}. Fig. 11(a) depicts spectrograms of $\Delta A(\omega, t)$ at the photon energy of 2.96, 3.13 and 3.30 eV. To obtain the dynamic information in detail, peak tracking analysis was

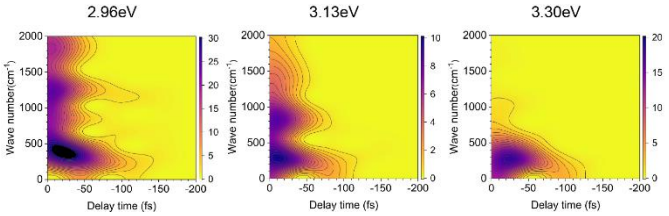

Fig. 12 Spectrogram of ΔA(ϖ,t) in negative time at photon energies of 2.96, 3.13 and 3.30 eV, respectively.

applied to high-frequency vibrational modes such as 1240 and 1400 cm^{-1} at 2.96 eV, 1370 cm^{-1} at 3.13 eV and 1230 and 1470 cm^{-1} at 3.30 eV. Although the instantaneous frequency is almost constant even when tracking the maximum intensity, the time trace of the instantaneous intensity of each vibrational mode at each photon energy shows oscillation (Fig. 11(b)). To clarify the modulation component, FFT was applied (Fig. 11(c)). The 1240 and 1400 cm^{-1} vibrational modes at 2.96 eV exhibit modulation values of 37, 98 and 160 cm^{-1} and 58, 98 and 160 cm^{-1}, respectively; 1370 cm^{-1} at 3.13 eV exhibits modulation frequencies of 55 cm^{-1} and 1230 and 1470 cm^{-1} at 3.30 eV exhibit modulation values of 48 and 85 cm^{-1} and 78 cm^{-1}, respectively. These low-frequency modes agree well with *ab initio* calculations. In addition, these are consistent with the simulated vibronic transition, i.e. the transition table involves the coupling of high- and low-frequency modes (see Table 1). Interestingly, although high-frequency modes considered here show in-plane motion, these low vibrational modes represent out-of-plane motions (see † ESI). Therefore, the coupling between low and high frequency modes induces symmetry-breaking behaviour during the relaxation process. This symmetry-breaking behaviour is a key factor in singlet fission materials to accelerate the fission dynamics.[73]

Fig. 12 shows the spectrograms of $\Delta A(\omega, t)$ in negative times at 2.96, 3.13 and 3.30 eV. From these spectra, we also found both high and low vibrational modes such as 317 and 1250 cm^{-1}, along with the electronic dephasing time in tetracene. Because the PFID process is a non-rephasing process in the electronically excited state, these vibrational coupling dynamics reflect the excited state dynamics, particularly dephasing dynamics.

Conclusions

Ultrafast dynamics of tetracene molecules in THF solution have been investigated using sub-8-fs UV pulse lasers. The time trace of absorbance changes exhibited an ultrafast decay component with a time constant of 165 ± 10 fs around a photon energy of 3.13 eV due to the relaxation from the vibronically hot excited state to the potential minimum in the S_1 state. By global fitting with 165 fs to create DAS, the fast component in DAS exhibited first derivative-like spectra of stationary absorption spectra. The slow component showed the reverse shape of the stationary absorption spectra with significantly broader bandwidth due to the hot band after photoexcitation. The electronic dephasing time derived from the absorbance change date in the negative time region could be estimated to be 31.27± 1.63 fs. Inverse Fourier transform of stationary absorption spectra showed rapid decay with a 2.1 ± 0.08 fs time constant with 24.3fs period (1430 cm^{-1}) oscillation. From these data, because the population decay time in the S_1 state is sufficiently long, we estimated the ratio of total dephasing time to homogenous and inhomogeneous broadening as 6.7% and 93.3%, respectively. Impulsive Raman spectra reflect the wave packet dynamics of vibrational modes. Although the inhomogeneous broadening obscured the phase jump across the resonance spectrum, the 1156 and 1680 cm^{-1} vibrational modes exhibited a phase jump from about $-\pi$ to ~π and -0.5π to ~0.5π, respectively. The amplitude profiles of these vibrational modes did not exhibit any typical dip at the resonance position; however, the experimental results were accurately reproduced by the simulated vibronic progressions that generated combination bands in the stationary absorption spectra. Time–frequency analysis by spectrograms revealed coupling dynamics between low and high frequency modes. The high frequency modes were in-plane motions, whereas the low frequency modes were out-of-plane motions. Therefore, these coupling dynamics induced molecules symmetry-breaking motion that could accelerate the singlet fission process.

Complementary to the experimental findings, *ab initio* calculations were also performed in this study. Vibronic spectra and resonance Raman spectra of tetracene molecules in THF solution could be reproduced well with high accuracy. For high accuracy, precise coupling dynamics were discussed, particularly mode mixing during the transition. Because the experimental absorption spectra exhibited broad bandwidth, the precise transition could not be observed. Thus, precise simulations facilitate correct interpretation.

Many interesting findings in the ultrafast spectroscopy of tetracene in THF solution were clarified. Crystals and/or thin films of tetracene will be investigated with this system in future studies.

Conflicts of interest

There are no conflicts to declare.

Acknowledgements

This work was supported by JSPS KAKENHI Grant Numbers 18K05048 and 21H01055 and partially supported by RIKEN-Osaka University Science and Technology Hub Collaborative Research Program for T. Teramoto. This work is also supported by the National Nature Science Foundation of China No. 61875211, CAS Interdisciplinary Innovation Team for J. Du. We are also grateful for the use of the HOKUSAI-GreatWave supercomputer system of RIKEN. The research described in this paper is partly an extension of the support provided by the following scheme of JST International Cooperative Research Project(ICORP) “Ultrashort Pulse Laser” project (Japan–Germany,2006–2011) conducted collaboratively by Professor Kobayashi (Professor of the University of Tokyo) and Professor

Ferenc Krausz (Director of Ultrakurz pulse laser group in Max Planck Institut).

Notes and references

1 AArmin, W.Li, O.J. Sandberg, Z.Xiao, L.Ding, J.Nelson, D.Neher, K.Vandewal, S. Shoaee, T.Wang, H.Ade, T.Heumüller, C.Brabec, and P.Meredith, *Adv. Energy Mater.,* 2021, **11**, 20003570.

2 A.Hagfeldt, G.Boschloo, L.Sun, L.Kloo, and H.Pettersson, *Chem. Rev.,* 2010,**110**, 6595−6663.

3 S.Günes,H.Neugebauer, and N.S.Sariciftci, *Chem. Rev.,*2007,**107**, 1324−1338.

4 M.A. Green, A.Ho-Baillie and H.J. Snaith, *Nat.Photon.*, 2014, **8**, 506−514.

5 C.Li, J.Zhou, J.Song, J.Xu, H.Zhang, X. Zhang, J.Guo, L.Zhu, D.Wei, G.Han, J.Min, Y.Zhang, Z.Xie, Y.Yi, H.Yan, F.Gao, F.Liu and Y.Sun, *Nat.Energy*,2021,**6**,605−613.

6 J.Jeong, M.Kim, J.Seo, H.Lu, P.Ahlawat, A. Mishra, Y.Yang, M. A. Hope, F.T. Eickemeyer, M.Kim, Y.Jin Yoon, I.W.Choi, B.P.Darwich, S.J.Choi, Y.Jo, J.H.Lee, B. Walker, S.M. Zakeeruddin, L.Emsley, U.Rothlisberger,A.Hagfeldt, D.S.Kim, M. Grätzel and J.Y.Kim, *Nature*,2021, **592** ,381−385.

7 M.J. Y. Tayebjee, D.R. McCamey, and T.W. Schmidt, *J. Phys. Chem. Lett.,* 2015, **6**, 2367−2378.

8 J.Lee, P.Jadhav, P.D. Reusswig, S.R. Yost, N.J. Thompson, D. N. Congreve, E.Hontz, T.Van Voorhis, and M.A. Baldo, *Acc. Chem. Res.,*2013, **46**,1300–1311.

9 A.Rao and R.H. Friend, *Nat. Rev. Mater.,* 2017, **2**, 17063.

10 J.Xia, S.N. Sanders, W.Cheng, J.Z. Low, J.Liu, L.M. Campos, and T.Sun, *Adv. Mater.* , 2017, **29**, 1601652.

11 M.Einzinger, T.Wu, J.F. Kompalla, H.L. Smith, C.F. Perkinson, L.Nienhaus, S. Wieghold, D.N. Congreve, A.Kahn, M.G. Bawendi and M.A. Baldo, *Nature*,2019, **571**, 90–94.

12 W.Shockley and H.J.Queisser, *J. Appl. Phys.* 1961, **32**, 510–519.

13 M.B. Smith and J.Michl,*Chem. Rev.,*2010, **110**, 6891–6936.

14 M.B. Smith and J.Michl, *Annu. Rev. Phys. Chem.,*2013, **64**,361–386.

15 D.Casanova, *Chem. Rev.*, 2018,**118**, 7164−7207.

16 D.N. Congreve, J.Lee, N.J. Thompson,E.Hontz, S.R. Yost,P. D. Reusswig, M.E. Bahlke, S.Reineke, T.V.Voorhis,and M.A. Baldo, *Science*,2013,**340**,334−337.

17 R.J. Hudson, A.N. Stuart, D.M. Huang, and T.W. Kee, *J. Phys. Chem. C* ,2022,**126**, 5369−5377.

18 S. Singh, W.J. Jones, W. Siebrand, B. P. Stoicheff, and W. G. Schneider, *J. Chem. Phys.,*1965, **42**, 330−342.

19 S.R. Ellis, D.R. Dietze, T.Rangel, F.Brown-Altvater, J.B. Neaton, and R. A. Mathies, *J. Phys. Chem. A,* 2019,**123**, 3863−3875.

20 A.A. Bakulin, S.E. Morgan, T.B. Kehoe, M.W. B. Wilson, A.W. Chin, D. Zigmantas, D.Egorova and A.Rao,*Nat. Chem.,*2016, **8**,16−23.

21 A.F. Morrison and J.M. Herbert, *J. Phys. Chem. Lett*.,2017, **8**, 1442−1448.

22 P.M. Zimmerman, F.Bell, D.Casanova, and M.Head-Gordon,*J. Am. Chem. Soc.,* 2011,**133**, 19944−19952.

23 W.Chan, M.Ligges and X.Y. Zhu,*Nat.Chem.,* 2012,**4**, 840.

24 C.Keong Yong, A.J. Musser, S.L. Bayliss, S.Lukman, H.Tamura, O.Bubnova, R. K. Hallani, A.Meneau, R.Resel, M.Maruyama, S.Hotta, L.M. Herz, D.Beljonne, J.E. Anthony, J.Clark and H.Sirringhaus, *Nat.Comm.,*2017, **8**,15953.

25 S. Lim,T.G. Bjorklund, F.C. Spano, and C. J. Bardeen, *Phys.Rev. Lett.* , 2004, **92**, 107402.

26 J.J. Burdett, A.M. Müller, D.Gosztola, and C.J. Bardeen, *J. Chem. Phys*., 2010, **133**, 144506.

27 W.Kim & A.J. Musser, *Adv.Phys.,* 2021, **6**, 1918022.

28 G.Wang, C.Zhang, Z.Liu, R.Wang, H.Ma, X.Wang, and M.Xiao, *J. Phys. Chem. A*, 2020,**124**, 10447−10456.

29 A.M. Müller, Y.S. Avlasevich, W.W. Schoeller, K.Müllen, and C.J. Bardeen, *J. Am. Chem. Soc.,* 2007,**129**, 14240−14250.

30 M.W. B. Wilson, A.Rao, K.Johnson, S.Gélinas, R.di Pietro, J.Clark, and R.H. Friend, *J. Am. Chem. Soc.,* 2013,**135**, 16680−16688.

31 B. Zhang, C.Zhang, R.Wang, Z.Tan, Y.Liu, W.Guo, X.Zhai, Y.Cao, X. Wang, and M.Xiao, *J. Phys. Chem. Lett.,*2014, **5**, 3462−3467.

32 Y.Wan, Z.Guo, T.Zhu, S.Yan, J.Johnson and L.Huang, *Nat. Chem.,* 2015, **7**,785−792.

33 A.J. Musser, M.Liebel, C.Schnedermann, T.Wende, T.B. Kehoe, A.Rao and P. Kukura, *Nat. Phys.,*2015, **11**,352−357.

34 S.Lim, T.G. Bjorklund, F.C. Spano, and C.J. Bardeen, *Phys.Rev.Lett.,*2004, **92**, 107402.

35 E.M. Grumstrup, J.C. Johnson, and N.H. Damrauer, *Phys.Rev.Lett.,* 2010, **105**, 257403.

36 Y.Wan, G.P. Wiederrecht, R.D. Schaller,J.C. Johnson, and L.Huang, *J. Phys. Chem. Lett.,* 2018,**9**, 6731−6738.

37 P.M. Zimmerman, C.B. Musgrave, and M.Head-gordon, *Acc. Chem. Res.* ,2013,**46**, 1339−1347.

38 H.Duan, A.Jha, X.Li, V.Tiwari, H.Ye, P.K. Nayak, X.Zhu, Z.Li, T.J. Martinez, M.Thorwart, and R. J. D. Miller, *Sci. Adv.,* 2020,**6** ,eabb0052.

39 C.Schnedermann, A.M. Alvertis, T.Wende, S.Lukman, J.Feng, F.A.Y.N. Schröder, D.H.P. Turban, J.Wu, N.D.M. Hine, N. C. Greenham, A.W. Chin, A.Rao, P. Kukura and A.J. Musser, *Nat. Comm.,*2019, **10**,4207.

40 B.A. West, J.M. Womick, L. E. McNeil, K. J.Tan, and A.M. Moran, *J. Phys. Chem. C*,2010,**114**, 10580−10591.

41 R. E. Merrifield, P. Avakian and R. P. Groff, *Chem.Phys.Lett.,* 1969, **3**,155−157.

42 G. B.Piland, and C. J.Bardeen, *J. Phys. Chem. Lett.,* 2015, **6**, 1841−1846.

43 J. J.Burdett,and C. J.Bardeen, *J. Am. Chem. Soc*.,2012, **134**, 8597−8607.

44 J.J. Burdett, D.Gosztola, and C.J. Bardeen, *J. Chem. Phys., 2011,* **135**, 214508.

45 Z.Birech, M.Schwoerer, T.Schmeiler, J.Pflaum, and H.Schwoerer, *J. Chem. Phys.*, 2014,**140**, 114501.

46 B.Zhang, C.Zhang, Y.Xu, R.Wang, B.He, Y.Liu, S.Zhang, X.Wang, and M. Xiao, *J. Chem. Phys.,*2014, **141**, 244303.

47 C.Zeiser, L.Moretti, F.Reicherter, H.F. Bettinger, M.Maiuri, G.Cerullo, and K.Broch, *ChemPhotoChem.,* 2021,**5**, 758−763.

48 V. K. Thorsmølle, R. D. Averitt, J. Demsar, D. L. Smith, S. Tretiak, R. L. Martin, X. Chi, B. K. Crone, A. P. Ramirez, and A. J. Taylor, *Phys.Rev.Lett.,* 2009,**102**, 017401.

49 J. Liu, Y.Kida, T.Teramoto, and T.Kobayashi, *Opt. Exp.,*2010, **18**, 4664−4672.

50 J. Liu, K.Okamura, Y.Kida, T.Teramoto, and T.Kobayashi, *Opt. Exp.* ,2010,**18**, 20645−20650.

51 J.Liu, A.Yabushita, S.Taniguchi, H.Chosrowjan, Y.Imamoto, K.Sueda, N. Miyanaga, and T.Kobayashi, *J. Phys. Chem. B,* 2013,**117**, 4818−4826.

52 Frisch, M. J., *et al.*, Gaussian 16, Wallingford, CT, https:// gaussian.com/citation/, 2016.

53 J.Du and T.Kobayashi, Chin.Opt.lett.,2011,**9**,S10601

54 C. Hsu, Y.Wang, A.Yabushita, C. Luo, Y. Hsiao, S. Lin, and T. Kobayashi, *J. Phys. Chem. A* 2011, **115**, 11508–11514.

55 C.H.B.Cruz, J.P.Gordon,P.C.Becker, R.L.Fork, and C.V. Shank, *IEEE J.Quantum.Electron.,1988,***24**,261−266.

56 M.Joffre,D.Hulin,A.Migus and A.Antonetti, *Opt.Lett*.,1988,**13**,276−278.

57 B. Fluegel, N. Peyghambarian, G. Olbright, M. Lindberg, S. W. Koch, M. Joffre, D. Hulin, A. Migus, and A. Antonetti,*Phys.Rev.Lett.*,1987,**59**,2588−2591.

58 T. Kobayashi, J.Du, W.Feng, and K.Yoshino, *Phys.Rev.Lett.*,2008, **101**,037402.

59 T.Teramoto, and T.Kobayashi,*Phys.Chem.Chem.Phys*.,2010, **12** , 13515−13518.

60 T.Kobayashi, Z.Nie, B.Xue, H.Kataura, Y.Sakakibara, and Y. Miyata, *J.Phys. Chem. C*, 2014,**118**, 3285−3294.
61 D.Han, B.Xue, J.Du, T.Kobayashi, T.Miyatake, H.Tamiaki, X.Xing, W.Yuan, Y.Lia and Y.Leng, *Phys. Chem. Chem. Phys.*,2016, **18**, 24252−24260.
62 R.L. Martin, *J. Chem. Phys.,* 2003,**118**, 4775−4777.
63 H.Kano, T.Saito, and T.Kobayashi,*J. Phys. Chem. A,* 2002,**106**, 3445−3453.
64 V. Barone, J. Bloino, and M. Biczysko, "Vibrationally-resolved electronic spectra in Gaussian 09" (2009), available online at http://dreamslab. sns.it/sites/default/files/download/docs/vibronic_spectra_G 09-A02.pdf"
65 A.T. N. Kumar, F.Rosca, A.Widom, and P.M. Champion, *J. Chem. Phys.,*2001, **114**, 701−724.
66 A.T. N. Kumar, F.Rosca, A.Widom, and P.M. Champion,*J. Chem. Phys*.,2001, **114**, 6795−6815.
67 T.Kobayashi, and A.Yabushita,*Chem.Rec*.,2011,**11**,99−116.
68 N. Ishii, E.Tokunaga, S.Adachi, T.Kimura, H. Matsuda, and T.Kobayashi, *Phys. Rev. A,* 2004,**70**, 023811.
69 J.Du, T.Teramoto, K.Nakata, E.Tokunaga, T.Kobayashi, *Biophys J.,* 2011,**101**,995−1003.
70 M. S. Barclay, J.S. Huff, R.D. Pensack, P.H. Davis, W.B. Knowlton,B.Yurke, J.C. Dean, P.C. Arpin, and D. B. Turner, *J. Phys. Chem. Lett.* 2022, **13**, 5413−5423.
71 A.Shimura, K.Yanagi, and M.Yoshizawa, *Phys. Rev. B*,2018, **97**, 035441.
72 L.Lüer, C.Gadermaier, J.Crochet, T.Hertel, D.Brida, and G.Lanzani, *Phys.Rev.Lett.* 2009,**102**, 127401.
73 S.Rafiq and G.D. Scholes, *J. Phys. Chem. A* 2016, **120**, 34, 6792–6799.
74 G.Batignani, C.Sansone, C.Ferrante, G.Fumero, S. Mukamel, and T.Scopigno,*J. Phys. Chem. Lett.* 2021, **12**, 9239−9247.
75 K.Miyata, Y. Kurashige, K.Watanabe, T.Sugimoto, S. Takahashi, S.Tanaka, J.Takeya, T.Yanai and Y.Matsumoto, *Nat. Chem.,* 2017,**9**, 983–989.